




Preparation of niobium-based oxygen carriers by polyol-mediated process and application to chemical-looping reforming

Pedro Henrique Lopes Nunes Abreu dos Santos · Sophie Nowak ·
Stephanie Lau-Truong · Juliette Blanchard · Patricia Beaunier ·
José Augusto Jorge Rodrigues · Roberta Brayner 

Received: 31 May 2018 / Accepted: 10 April 2019 / Published online: 1 May 2019
© Springer Nature B.V. 2019

Abstract New niobium-based oxygen carriers were prepared adopting polyol-mediated process. Four different polyols were used (diethylene glycol, triethylene glycol, tetraethylene glycol, and 1,2-propanediol) and four different quantities of water (0 mL, 1 mL, 10 mL, 30 mL, with a total volume of 80 mL of solution). Series of bulk and alumina-supported materials were prepared. Different structural and textural properties were obtained, depending on polyol type and hydrolysis ratio. After thermal treatment at 1000 °C, alumina-supported materials were evaluated in a lab-scaled fixed bed reactor. Despite a low conversion of methane due to a low

content of active phase AlNbO_4 , they presented a high selectivity to syngas (a mixture of H_2 and CO) during the first few seconds of reaction with CH_4 , indicating a high selectivity towards chemical-looping reforming process.

Keywords Chemical-looping reforming · Polyol-mediated synthesis · Oxygen carrier · Niobia · Nanomaterials · Oxygen carrier

Introduction

Chemical looping is an excellent alternative technology for industrial processes that make use of fossil fuel, (Kvamsdal et al. 2007; Miracca et al. 2009; Adanez et al. 2012) such as combustion reactions that generate energy and reforming reactions that generate hydrogen. One of the best advantages of this technology is that it can capture the CO_2 that is inherently produced by these processes. Chemical-looping combustion (CLC) and chemical-looping reforming (CLR) use an oxygen carrier, a metal oxide which may be supported on an inert support matrix (alumina, for example) (Gayán et al. 2008; de Diego et al. 2005; Zafar et al. 2006) and have characteristics similar to that of an heterogeneous catalyst.

This oxygen carrier material circulates through two reactors: an air reactor and a fuel reactor, as seen in Fig. 1 (Adanez et al. 2012). When in contact with the fuel, the metal oxide provides oxygen. The reaction is

P. H. L. N. A. dos Santos
EEL-USP - Escola de Engenharia de Lorena, DEMAR -
Departamento de Engenharia de Materiais, Pólo-Urbo Industrial,
Universidade de São Paulo, Gleba AI-6, s/n, Lorena, SP
12602-810, Brazil

P. H. L. N. A. dos Santos · S. Nowak · S. Lau-Truong ·
R. Brayner (✉)
Sorbonne Paris Cité, Interfaces, Traitements, Organisation et
Dynamique des Systèmes (ITODYS), UMR 7086, CNRS,
Paris-Diderot University, 15 rue Jean de Baïf, 75205 Paris Cedex
13, France
e-mail: roberta.brayner@univ-paris-diderot.fr

P. H. L. N. A. dos Santos · J. A. J. Rodrigues
LCP - Laboratório Associado de Combustão e Propulsão, INPE -
Instituto Nacional de Pesquisas Espaciais, Rodovia Presidente
Dutra, KM 40, Cachoeira Paulista, SP 12630-000, Brazil

J. Blanchard · P. Beaunier
CNRS, Laboratoire de Réactivité de Surface, LRS, Sorbonne
Université, F-75005 Paris, France

either total oxidation (combustion) or partial oxidation (reforming). When the material enters the air reactor, it is either partially or totally reduced. There, it is reoxidized, leading to a continuous process of combustion or reforming of the fossil fuel.

Chemical-looping technology is still under development. There are many technological challenges ahead before it can be implemented, such as the need to scale up the reactors that are currently used in oxygen carrier studies. In the specific case of the CLR process, one of the technological challenges that limits its development is finding an oxygen carrier that is highly selective to the reforming reaction at high temperatures (the process normally takes place between 800 and 1000 °C).

Niobium oxide

Over the past few years, the scientific community has begun to consider niobium oxide as a good alternative in heterogeneous catalysis (Tanabe 2003; Ziolk 2003) because it is acidic and has redox and photocatalytic properties. Nb has different oxidative states from -1 to $+5$. It can form NbO , Nb_2O_3 , NbO_2 , and Nb_2O_5 oxides. Nb_2O_5 is the most common, the Nb^{+5} oxidation state being the most stable (Nowak and Ziolk 1999).

Different thermal treatments can cause Nb_2O_5 to develop different crystalline structures. The most

common phases are amorphous Nb_2O_5 , TT- Nb_2O_5 (pseudo-hexagonal structure), T- Nb_2O_5 (orthorhombic structure), and H- Nb_2O_5 (monoclinic structure) (Ko and Weissman 1990). Many studies have been carried out regarding the application of this oxide in heterogeneous catalysis, with the aim of taking advantage of this crystallographic versatility. Niobium oxide can be used as a support (Li et al. 2004; Mozer and Passos 2011), promoter (Chun et al. 2010), or even as active phase (Li et al. 2005; He et al. 2013) in a catalyst. It can even influence the properties of known catalysts, increasing their life cycle and/or reactivity (Tanabe 2003).

The polyol process

Another scientific area that has recently attracted increasing attention is the study of nanostructured materials. These materials are promising in the area of heterogeneous catalysis because they have not only higher surface areas, but also different properties than bulk materials due to quantum size effects that allow controlling their band gap.

Several groups have explored different methods for the synthesis of nanostructured niobium oxide, producing materials with different particle sizes and morphologies (Zhao et al. 2012). In this study, we have adopted the polyol method, in which a salt precursor of the oxide is solubilized in a α -diol or a glycol ether to which a small amount of water is added. Under these conditions, the oxide is synthesized through forced hydrolysis, similar to the sol-gel process. The solvent has a large number of hydroxyl groups that strongly interact with the surface of the particle during its formation, and in the end, a nanostructured particle with controllable shape and dimension is obtained (Fiévet and Brayner 2013).

The objective of this study is to synthesize and characterize niobium oxides prepared from a polyol process (with or without an alumina support) and to evaluate the applicability of the supported and calcined materials in the CLR process.

Experimental

Preparation

Commercial Nb_2O_5 (HY-340) and the precursor ammonium niobate oxalate were supplied by CBMM (Companhia Brasileira de Metalurgia e Mineração,

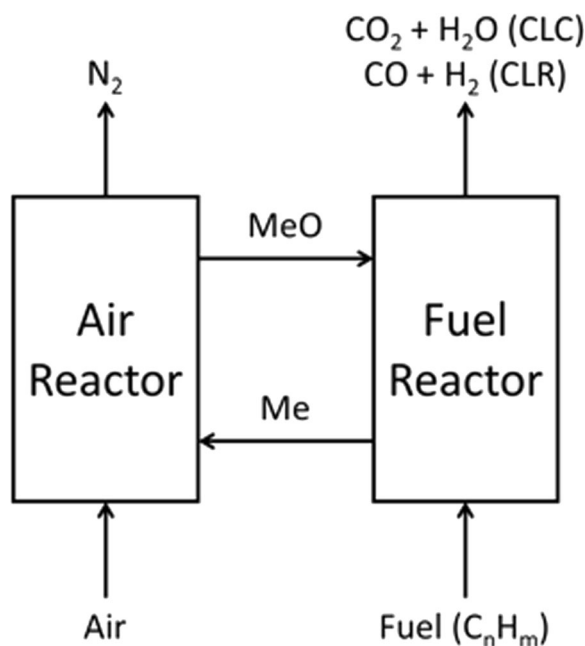


Fig. 1 Diagram of the interconnected reactors

Brazil); the alumina (Puralox NWA 155) was kindly provided by Sasol (Germany).

Synthesis was carried out in two different ways. Niobium oxide was prepared with and without an alumina support. For synthesis without the support, the oxides were prepared by the hydrolysis of 1 g of ammonium niobate oxalate in a polyol medium using a small quantity of zinc acetate (0.0015 g) as nucleant. Four different polyols were used: diethylene glycol (DEG), triethylene glycol (TEG), tetraethylene glycol (TTG), and 1,2-propanediol (1,2PD). Different amounts of water were added to induce the hydrolysis process, always maintaining a total volume of 80 mL. For the preparation of the supported materials, ammonium niobate oxalate and alumina were added to the polyol/water mixture, so as to produce 5 wt% Nb₂O₅/Al₂O₃ samples. The water/polyol ratios were identical to those used for the synthesis of the unsupported samples. Reference code of each sample is related to their synthesis parameters. Table 1 shows the relation between reference code and synthesis parameters.

The suspensions were maintained for both series of materials under stirring. The mixtures were then heated to the boiling point of the polyol-water mixture. This temperature varies over a wide range of values depending mostly on the volume of water in the solution and also on the polyol type (see Table 1 for temperature values). These conditions were maintained for 3 h with reflux. The resulting materials were centrifuged, washed with ethanol, and dried at 50 °C. Supported materials were calcined, in order to stabilize this material for evaluation tests, to 1000 °C for 3 h, using a heating rate of 3 °C/min, under air in a furnace. When calcined, samples receive a “C” at the end of their reference (for example, sample prepared with diethylene glycol, with 10 mL of water and supported (DEG 10 Al), when calcined, is called DEG 10 Al C). Table 1 shows sample names and their synthesis conditions adopted.

Characterizations

Materials were characterized by X-ray diffraction (PANalytical X'PertPRO, with CoK α radiation, in the range of 10° < 2 θ < 80°), transmission electron microscopy (TEM) observations, and EDS X-ray microanalysis were carried out on a JEOL JEM 2100Plus transmission electron microscope, operating at 200 kV, interfaced to Oxford Instruments AZtec EDS system with an X-Max T large area (80 mm²) SDD detector,

UV-visible diffuse reflectance (Perkin Elmer Lambda 1050), nitrogen adsorption (surface area calculated by the BET method, Quantachrome Nova 2200), and thermogravimetry with differential thermal analysis (SETARAM). TG-DTA analyses were carried out in an air atmosphere from room temperature to 950 °C at a heating rate of 10 °C/min. Acidity was evaluated by FTIR of adsorbed pyridine. FTIR spectra were obtained on a Bruker Vector 22 FT-IR spectrometer (resolution, 4 cm⁻¹). Samples were pressed into self-supported wafers (ca. 10 mg/cm²) and heated at 400 °C for 2 h in O₂ (PO₂ = 13.3 kPa). They were evacuated afterward for 1 h at this temperature. Pyridine (*P* = 133 Pa) was introduced at RT and spectra were recorded after thermal desorption either at 150 or at 350 °C. Only Lewis acid sites were detected. The number of Lewis acid sites remaining after thermal treatment at 150 °C (corresponding to weak and strong Lewis sites) and after thermal treatment at 300 °C (corresponding to strong Lewis sites) was calculated by measuring the area of the band at 1454 cm⁻¹ after thermal treatment at these two temperatures and using the following equation (Barzetti et al. 1996; Kitano et al. 2012):

$$q_H = \frac{A_I \pi R^2}{w \varepsilon_I} \quad (1)$$

in which q_H is the concentration of acid sites in the sample; A_I is the area under the peaks in the IR analysis; R is the radius of the disk (0.8 cm); w is the mass of the sample; and ε_I is the absorption coefficient (2.22 cm/ μ mol for the band at 1454 cm⁻¹) (Emeis 1993).

In-situ XRD thermal analyses in an air atmosphere were conducted on non-supported materials prepared with 10 mL H₂O and supported sample TTG 10 Al. The experiments were carried out from room temperature to 950 °C. The XRD profiles were obtained in all temperatures with 100° steps.

Evaluation

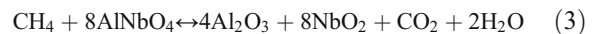
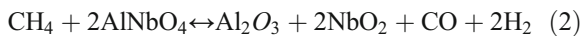
Supported oxygen carriers calcined at 1000 °C were evaluated in the CLR process. In a CLR process, two reactors are used: a fuel reactor and an air reactor. To simulate this set-up, reduction cycles with methane and reoxidation cycles with oxygen were carried out in a single reactor (in quartz) at 950 °C. One gram of supported oxygen carrier was used with a total gas flow of 50 mL/min, under atmospheric pressure. The gas

Table 1 Sample names and synthesis parameters

Sample reference	Polyol	Supported	H ₂ O volume (mL)	Reaction temperature (°C)			
DEG 01	DEG	No	1	216			
DEG 10			10	133			
DEG 30			30	106			
DEG 00 Al		Yes	Yes	0	245		
DEG 01 Al				1	213		
DEG 10 Al				10	134		
DEG 30 Al				30	106		
TEG 01				TEG	No	1	254
TEG 10						10	126
TEG 30	30	105					
TEG 00 Al	Yes	Yes	0		273		
TEG 01 Al			1		216		
TEG 10 Al			10		124		
TEG 30 Al			30		105		
TTG 01			TTG		No	1	260
TTG 10						10	122
TTG 30	30	103					
TTG 00 Al	Yes	Yes		0	280		
TTG 01 Al				1	225		
TTG 10 Al				10	124		
TTG 30 Al				30	103		
1,2PD 10				1,2PD	No	10	124
1,2PD 30						30	107
1,2PD 00 Al	Yes	Yes	0			187	
1,2PD 01 Al			1		173		
1,2PD 10 Al			10		128		
1,2PD 30 Al			30		107		

contained 10% CH₄ for the reduction step and 10% O₂ for the oxidation step. The remainder of the gas was argon in both cases. Reaction times were set at 6 min for the reduction step and 12 min for the oxidation step.

The reaction products were analyzed with an MKS e-Vision+ mass spectrometer and by a Varian CP-3800 gas chromatograph. The results were evaluated considering the selectivity of the CLR and CLC processes, carbon deposit on the surface of the material, and methane conversion throughout the reaction. Reactions represented in equations from 2 to 4 were considered to calculate selectivities and conversion.



From these reactions, several hypotheses should be made:

- According to Eq. 2, all CO formed can be related to CLR reaction (1 mol of CO/mol of CH₄);
- According to Eq. 3, all CO₂ formed can be related to CLC reaction (1 mol of CO₂/mol of CH₄);
- According to Eq. 4, carbon deposition can be estimated by subtracting to total H₂ formed, the fraction of H₂ formed according to Eq. 2 (2 mol H₂/mol CO). Equation 5 can be written:

$$[H_{2(Dep.C)}] = [H_2] - [H_{2(CLR)}] \tag{5}$$

where $[H_2]$ is the total hydrogen produced and $[H_{2(CLR)}]$ is the hydrogen produced from Eq. 2. $[H_{2(CLR)}]$ can be estimated as:

$$[H_{2(CLR)}] = 2[CO] \tag{6}$$

where $[CO]$ is the total amount of CO produced. Then the contribution from carbon deposition could be estimated as:

$$Dep.C \propto \frac{[H_{2(Dep.C)}]}{2} = \frac{[H_2]}{2} - [CO] \tag{7}$$

CLC and CLR contributions could be estimated as:

$$CLC \propto [CO_2] \tag{8}$$

$$CLR \propto [CO] \tag{9}$$

Then, selectivities can be calculated as:

$$S_{CLC} = \frac{CLC}{CLC + CLR + Dep.C} \tag{10}$$

$$S_{CLR} = \frac{CLR}{CLC + CLR + Dep.C} \tag{11}$$

$$S_{Dep.C} = \frac{Dep.C}{CLC + CLR + Dep.C} \tag{12}$$

Conversion of methane could be calculated as:

$$C_{CH_4} = \frac{CLC + CLR + Dep.C}{CLC + CLR + Dep.C + [CH_{4(not\ reacted)}]} \tag{13}$$

where $[CH_{4(not\ reacted)}]$ is the amount of CH_4 not reacted, directly identified from evaluation curves.

Results and discussion

Non-supported samples

Table 2 shows the main characterization results obtained for these samples.

Variation in the volume fraction of water has some influence on the structure of the material, as seen in

Fig. 2, which shows the X-ray diffraction profiles of uncalcined samples prepared using various water/ tetraethylene glycol (TTG series) ratios (see Table 1 for details). Materials prepared with 10 and 30 mL of water presented $HNbO_3$ phase (ICDD card 00-036-0794). On the other hand, materials prepared with 1 mL of water appears to have an amorphous structure, similar to that observed for commercial oxide HY 340. This could indicate that an increase in water volume can lead to materials with more organized structures. The diffraction profiles of materials prepared with 10 mL and 30 mL of water show that with even larger amounts of water, the material begins to have a slightly less ordered structure (the peaks on the material prepared with 10 mL of water are slightly better defined than those of the material prepared with 30 mL of water).

TG-DTA together with in situ XRD profiles recorded during thermal treatment reveal the transformations that take place in the materials as the temperature increases.

TG curves of a series of non-supported material prepared with 10 ml of water in the reaction mixture and using various polyols are reported in Fig. 3a. On all curves, there are two main regions of mass loss: the first is from room temperature to ca. 170 °C and the second is between ca. 170 and 300 °C. The DTA curves (Fig. 3b) show that the first mass drop corresponds to an endothermic event (and is therefore likely due to the loss of hydration water). The second drop occurs at slightly different temperatures depending on the polyol and has different heat releases (in the case of samples TEG 10 and TEG 30, not shown, there are no large variations in energy associated with this second mass loss). A third mass loss can be seen for most samples between 550 and 620 °C. It is weaker than the second mass loss and associated with an exothermic peak.

The in situ XRD profiles recorded during calcination reveal modifications to the crystalline structure at temperatures of 300 °C, 600 °C, 800 °C, and 950 °C, as seen in Fig. 4.

At a temperature of 300 °C, the first change in the structure of the materials takes place, with the loss of the diffraction lines of the $HNbO_3$ phase. The alteration coincides with the loss of mass seen in the TG curves between 170 and 300 °C. This mass loss can be only partially explained by the decomposition of $HNbO_3$ into amorphous niobium oxide ($Nb_2O_5 \cdot nH_2O$). Indeed, decomposition of $HNbO_3$ in $Nb_2O_5 \cdot nH_2O$ can represent a maximum mass loss of approximately 6% (considering $n = 0$). However, as it can be seen, the mass loss for all

Table 2 Non-supported materials main characterization results

Sample	Crystalline phase ⁽¹⁾	Weight loss (%) ⁽²⁾	E_g (eV) ⁽³⁾	A_S (m ² /g) ⁽⁴⁾	D_p (nm) ⁽⁵⁾	V_p (cm ³ /g) ⁽⁵⁾
DEG 01	25 °C: HNbO ₃	25–200 °C, 14.2 200–1000 °C, 11.9	3.1	345	3.4	0.177
DEG 10	25 °C: HNbO ₃ 300 °C: Nb ₂ O ₅ (amorphous) 600 °C: Nb ₂ O ₅ (pseudo-hexagonal) 800 °C: Nb ₂ O ₅ (orthorhombic) 950 °C: Nb ₂ O ₅ (monoclinic)	25–160 °C, 7.7 160–1000 °C, 34.0	2.5	4	–	–
DEG 30	25 °C: HNbO ₃	25–180 °C, 9.9 180–1000 °C, 22.7	2.9	197	3.4	0.142
TEG 01	25 °C: HNbO ₃	25–150 °C, 6.3 150–1000 °C, 20.1	3.3	156	–	0.101
TEG 10	25 °C: HNbO ₃ 300 °C: Nb ₂ O ₅ (amorphous) 600 °C: Nb ₂ O ₅ (pseudo-hexagonal) 800 °C: Nb ₂ O ₅ (orthorhombic) 950 °C: Nb ₂ O ₅ (monoclinic)	25–170 °C, 9.8 170–1000 °C, 21.4	3.0	64	–	–
TEG 30	25 °C: HNbO ₃	25–180 °C, 9.4 180–1000 °C, 15.6	3.0	144	–	–
TTG 01	25 °C: Nb ₂ O ₅ (amorphous)	25–200 °C, 6.6 200–1000 °C, 13.5	3.1	332	–	0.110
TTG 10	25 °C: HNbO ₃ 300 °C: Nb ₂ O ₅ (amorphous) 600 °C: Nb ₂ O ₅ (pseudo-hexagonal) 800 °C: Nb ₂ O ₅ (orthorhombic) 950 °C: Nb ₂ O ₅ (orthorhombic)	25–160 °C, 6.3 160–1000 °C, 27.0	3.1	49	–	–
TTG 30	25 °C: HNbO ₃	25–180 °C, 5.9 180–1000 °C, 20.3	2.8	37	–	–
1,2PD 10	25 °C: HNbO ₃ 300 °C: Nb ₂ O ₅ (amorphous) 600 °C: Nb ₂ O ₅ (pseudo-hexagonal) 800 °C: Nb ₂ O ₅ (orthorhombic) 950 °C: Nb ₂ O ₅ (monoclinic)	25–160 °C, 8.5 160–1000 °C 27.0	2.8	171	3.3	0.134
1,2PD 30	25 °C: HNbO ₃	25–180 °C, 12.2 180–1000 °C, 18.1	2.8	198	3.4	0.145

(1) Obtained by XRD analysis, (2) Obtained by TG-DTA; (3) Obtained by UV-visible diffuse reflectance analysis; (4) Obtained by nitrogen volumetry adopting BET treatment; (5) Obtained by nitrogen volumetry adopting BJH treatment

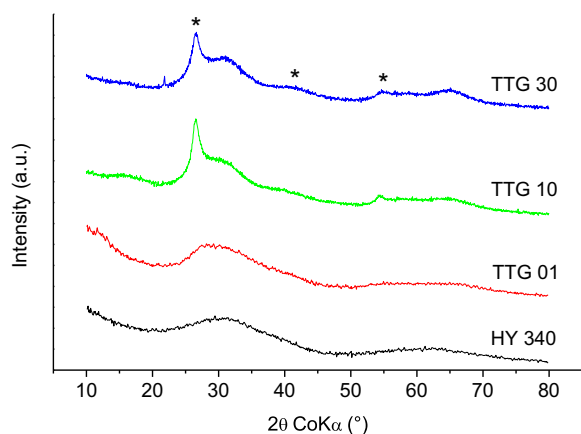


Fig. 2 X-ray diffraction profiles of unsupported samples before calcination: TTG 01 (red), TTG 10 (green), and TTG 30 (blue). The profile of a commercial Nb₂O₅ sample (HY 340, black) is also shown, for comparison. The lines identified as HNbO₃ phase (ICDD card 00-036-0794) are marked with an asterisk

samples is higher than 20%. Another event that could be happening at the same time is the thermal decomposition of the small part of polyol that had not been eliminated during washing step. The decomposition of polyols could explain why this second weight loss do not occur at the exact same temperature for samples prepared with different polyols. A similar weight loss has previously been reported by Li et al. (2016) during thermal treatment of niobium oxohydroxide prepared in ethanol and assigned to the decomposition of adsorbed organic molecules. The identification of the niobium oxide phase present after thermal treatment at 300 °C is not possible as the peaks are very broad and lack intensity. This is thought to be an indication that an amorphous structure of the oxide Nb₂O₅ forms after 300 °C. Another event that takes place at this temperature is the appearance of sharp peaks, which are due to the corundum wafer on which the sample had been

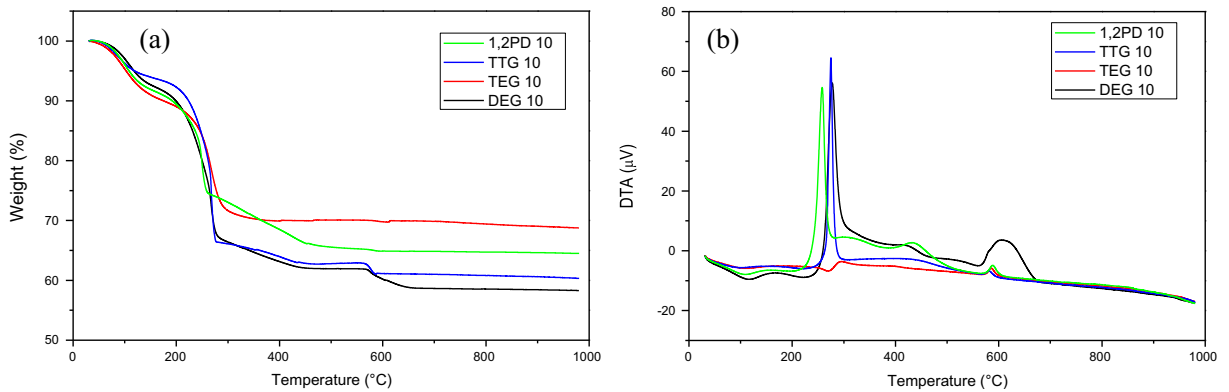


Fig. 3 Thermogravimetric analysis of uncalcined non-supported samples: DEG 10 (black), TEG 10 (red), TTG 10 (blue), and 1,2PD 10 (green). **a** TG profiles. **b** DTA profiles

deposited for measurement. Because of the mass loss, a contraction of the sample has occurred, leading the exposure of the corundum wafer to the X-ray beam.

The second modification takes place at 600 °C, where Nb₂O₅ with a pseudo-hexagonal structure, is observed (ICDD card 00-028-0317). This transformation coincides with the thermal event in the DTA curves between 550 and 620 °C discussed above. The third changed is observed after thermal treatment at 800 °C, where the structure changes from pseudo-hexagonal to

orthorhombic (ICDD card 00-30-0873). Figure 5 shows an enlargement (in the 30-45° 2θ range) of the diffraction profiles recorded after thermal treatment at 600 and 800 °C: the phase transformation is evidenced by the splitting of the diffraction lines on the profile recorded after thermal treatment at 800 °C.

These results agree with data from Ko et al. who investigated the thermal transformations of Nb₂O₅ (Ko and Weissman 1990). According to the work of these authors, the low temperature phase (pseudo-hexagonal

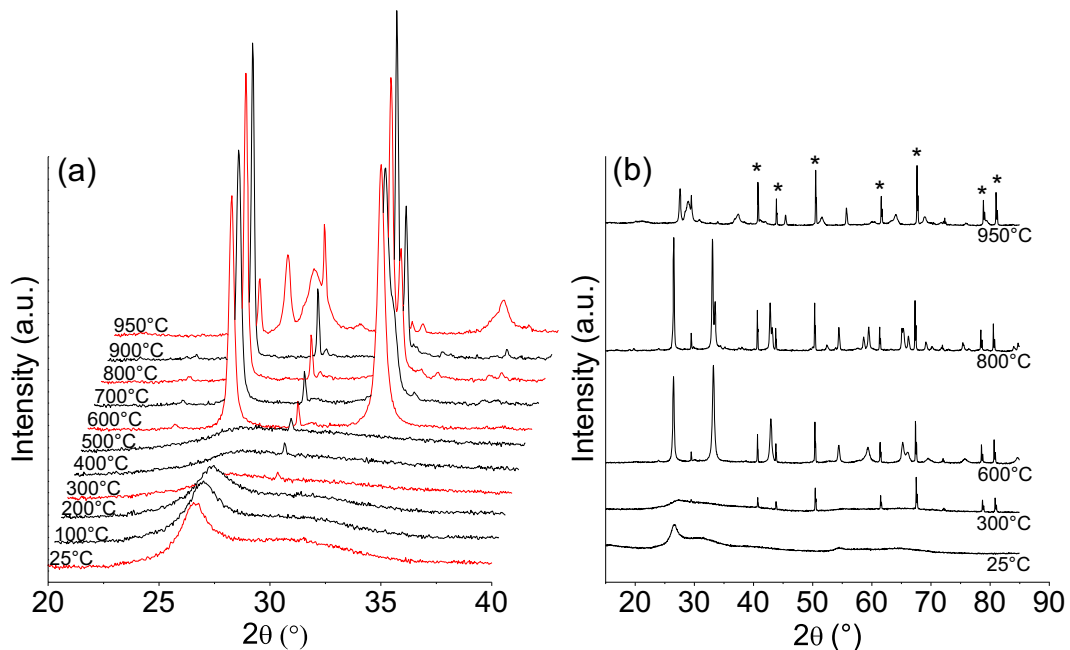
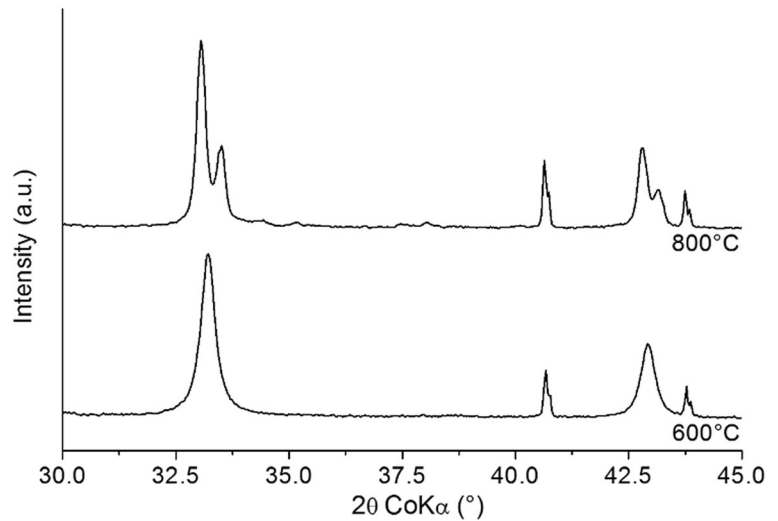


Fig. 4 In situ XRD analysis of TEG 10. **a** Diffraction profiles (between 2θ = 20 and 2θ = 40°) at all temperatures analyzed and **b** full diffraction profiles at structural modification temperatures (corresponding to profiles in red on (a) (the peaks marked with

an asterisk correspond to the corundum phase and are due to the corundum wafer on which the sample is deposited for the in situ XRD measurement)

Fig. 5 Diffraction profiles in the $30\text{--}45^\circ 2\theta$ range recorded at 600°C (with diffraction lines characteristic of the pseudo-hexagonal structure) and at 800°C (with diffraction lines characteristic of the orthorhombic structure). Sample: TEG 10



structure, called $\text{TT-Nb}_2(\text{O},\text{Y})_{5+n}$) and intermediate temperature phase (orthorhombic structure, called $\text{T-Nb}_2\text{O}_5$) have similar crystallographic structures but differ by the fact that the $\text{TT-Nb}_2(\text{O},\text{Y})_{5+n}$ phase contain

impurities (OH^- , for example). Due to these impurities in the $\text{TT-Nb}_2(\text{O},\text{Y})_{5+n}$, the Nb atoms can indifferently occupy two crystallographically similar sites, whereas, in the orthorhombic structure, they occupy either one or

Fig. 6 **a** TEM image and SAED pattern in insert. **b** EDX spectrum corresponding to TEG 10 sample

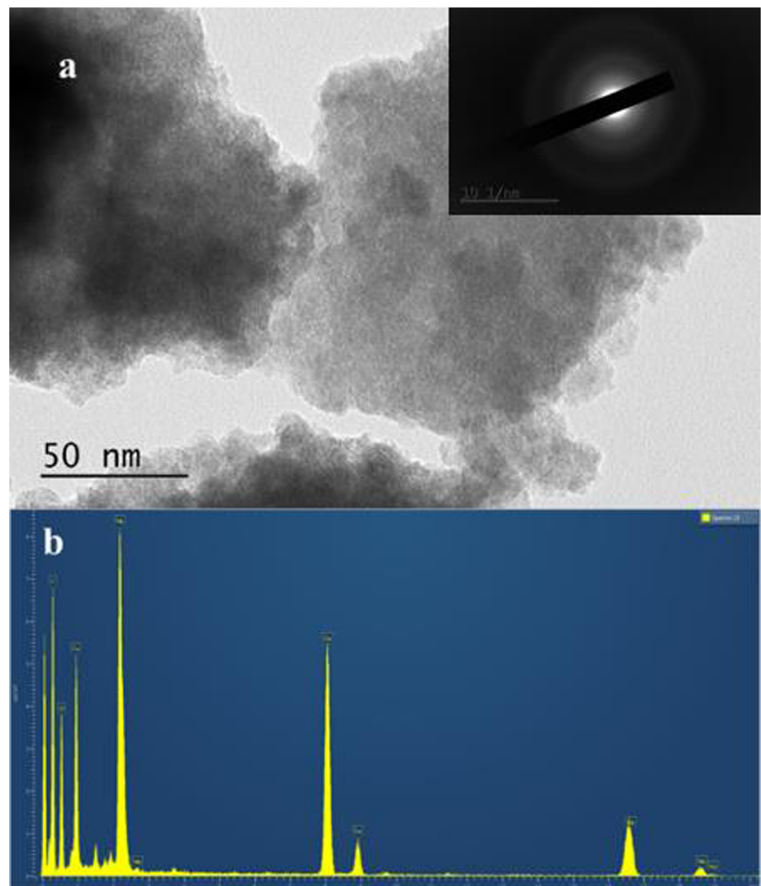
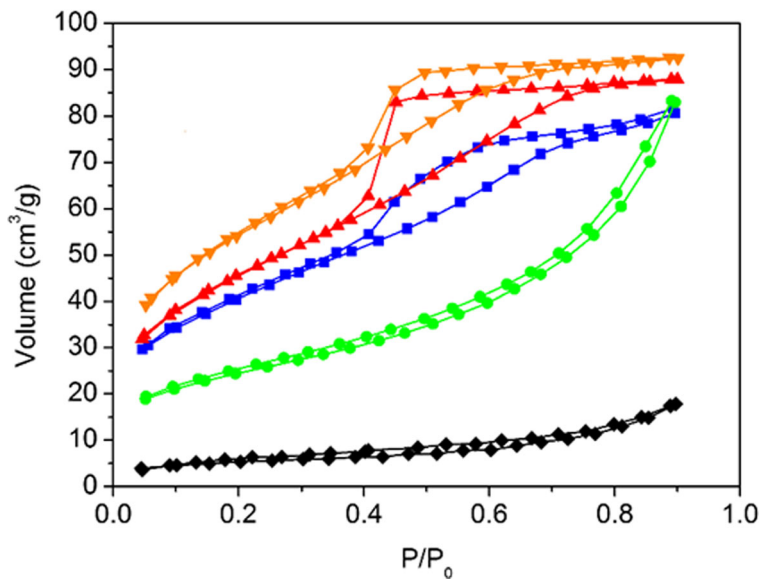


Fig. 7 N₂ adsorption–desorption profiles of non-supported and non-calcined materials prepared with 30 mL of water added to various polyols. (▲) DEG 30, (●) TEG 30, (◆) TTG 30, (▼) 1,2PD 30. The isotherm of commercial oxide (■) HY 340 is also shown for comparison



the other. This explains why the peaks for the pseudo-hexagonal structure are broader (and also the splitting of the peaks in the orthorhombic structure) (Ko and Weissman 1990).

The last change takes place at a temperature of 950 °C, when the monoclinic phase forms. This last transformation does not take place for sample TTG 10, which maintains the orthorhombic structure until 950 °C.

An interesting point is that we could not detect any signal in the DTA curves that would indicate modifications in the crystalline structure around 800 °C (transition from TT-Nb₂O₅ to T- Nb₂O₅) and around 950 °C (transition from T- Nb₂O₅ to H- Nb₂O₅).

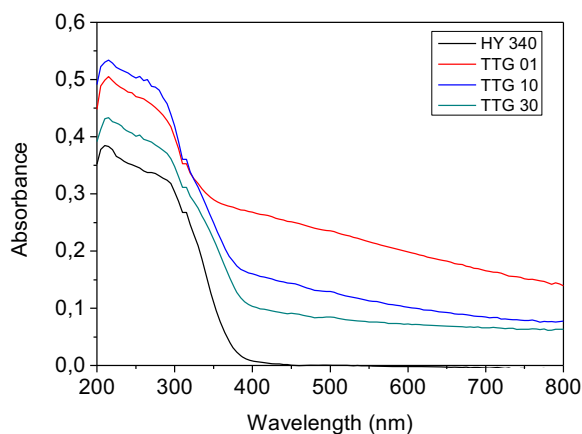


Fig. 8 UV-Vis spectra of a series of uncalcined non-supported materials prepared using tetraethylene glycol

Figure 6 a shows the high-resolution transmission electron microscopy (HRTEM) micrograph of the TEG 10 sample. We can see that the sample is amorphous (the SAED pattern in insert) which confirms the XRD result at 25 °C. Figure 6 b shows the elemental analysis (EDX) of the sample proving the presence of niobium and oxygen. The structural properties of the samples were also investigated by nitrogen physisorption. BET surface areas, pore sizes, and pore volumes for the non-supported samples are compiled in Table 2. The specific areas vary over a wide range of values, depending on the water volume and on the polyol, whereas the pore size distribution is almost identical when the same polyol is used. The N₂ adsorption-desorption isotherms of a series of samples prepared with various polyols and the same amount of added water (30 mL) are reported in Fig. 7. The samples prepared with triethyleneglycol (TEG) and tetraethyleneglycol (TTG) have type II isotherms according to IUPAC classification (IUPAC 1985, 1994), indicating that the materials prepared with these two polyols are not porous. The high surface area, which reached 332 m²/g for sample TTG 01, is related to the nano-scale size of the particle formed.

Materials prepared with 1,2-propanediol, as well as commercial oxide HY 340, present a combination of type I and type IV isotherms with a H2 type hysteresis loop, according to IUPAC classification (IUPAC 1985, 1994). These characteristics are indicative of a microporous and mesoporous structure with ink bottle-shaped

Table 3 Supported materials main characterization results (before calcination)

Sample	Crystalline phase ^(1,8)	E_g (eV) ^(3,7)	Nb ₂ O ₅ content ⁽⁶⁾	A_S (m ² /g) ⁽⁴⁾	D_P (nm) ⁽⁵⁾	V_P (cm ³ /g) ⁽⁵⁾
Support	γ -Al ₂ O ₃	—	—	146	7.0	0.350
DEG 00 Al	γ -Al ₂ O ₃	3.3	3.7	133	7.0	0.326
DEG 01 Al	γ -Al ₂ O ₃	3.8	4.1	128	7.0	0.305
DEG 10 Al	γ -Al ₂ O ₃	3.5	2.7	147	6.9	0.273
DEG 30 Al	γ -Al ₂ O ₃	3.6	3.5	142	7.0	0.307
TEG 00 Al	γ -Al ₂ O ₃	3.1	4.0	114	7.0	0.310
TEG 01 Al	γ -Al ₂ O ₃	3.7	3.8	130	8.1	0.316
TEG 10 Al	γ -Al ₂ O ₃	3.2	3.3	117	6.9	0.261
TEG 30 Al	γ -Al ₂ O ₃	3.2	3.8	135	7.0	0.300
TTG 00 Al	γ -Al ₂ O ₃	—	3.7	124	8.1	0.302
TTG 01 Al	γ -Al ₂ O ₃	3.2	3.6	134	7.0	0.312
TTG 10 Al	γ -Al ₂ O ₃	3.3	3.9	90	6.0	0.270
TTG 30 Al	γ -Al ₂ O ₃	3.3	3.9	90	7.0	0.315
1,2PD 00 Al	γ -Al ₂ O ₃	3.4	1.0	129	8.2	0.293
1,2PD 01 Al	γ -Al ₂ O ₃	3.7	1.6	131	6.9	0.246
1,2PD 10 Al	γ -Al ₂ O ₃	3.5	2.6	120	7.0	0.315
1,2PD 30 Al	γ -Al ₂ O ₃	3.4	3.5	140	7.0	0.297

⁽¹⁾ Obtained by XRD analysis, ⁽²⁾ Obtained by TG-DTA; ⁽³⁾ Obtained by UV-visible diffuse reflectance analysis; ⁽⁴⁾ Obtained by nitrogen volumetry adopting BET treatment; ⁽⁵⁾ Obtained by nitrogen volumetry adopting BJH treatment; ⁽⁶⁾ Obtained by ICP-OES (after calcination and assuming that every Nb atom went to Nb₂O₅ oxidized state)

⁽⁷⁾ Results obtained subtracting the alumina curve

⁽⁸⁾ Nb compounds crystalline phase not found by XRD analysis to supported material

isotherm. The average mesopores size, calculated by applying the BJH model to the adsorption isotherm is 3.3 nm.

The three samples prepared with diethylene glycol behaved differently, depending on the water content. Samples DEG 01 and DEG 30 had types I+II isotherms. Sample DEG 01 had a characteristic type H1

hysteresis characteristic of cylindrical pores, while sample DEG 30 had type H2 hysteresis, indicating that the pores had an “Ink Bottle” shape. Sample DEG 10 has a very small surface area, indicating the absence of meso- or micropores in this sample.

The UV-Vis spectra of a series of samples prepared without alumina support and using a solution of TTG

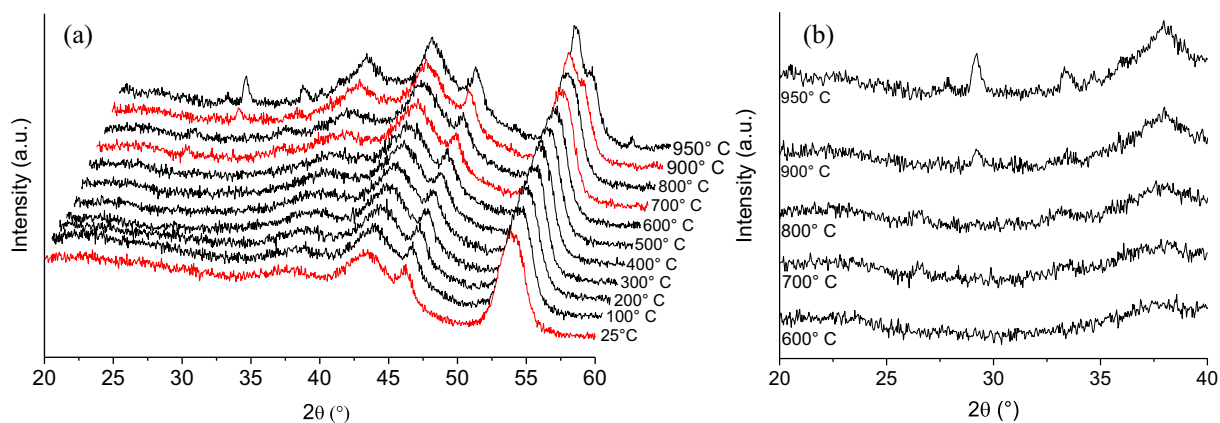


Fig. 9 **a** In situ XRD analysis of TTG 10 Al. Profiles in red: Temperatures where the crystalline structure has been modified. **b** Zoom between 20° and 40° (2θ)

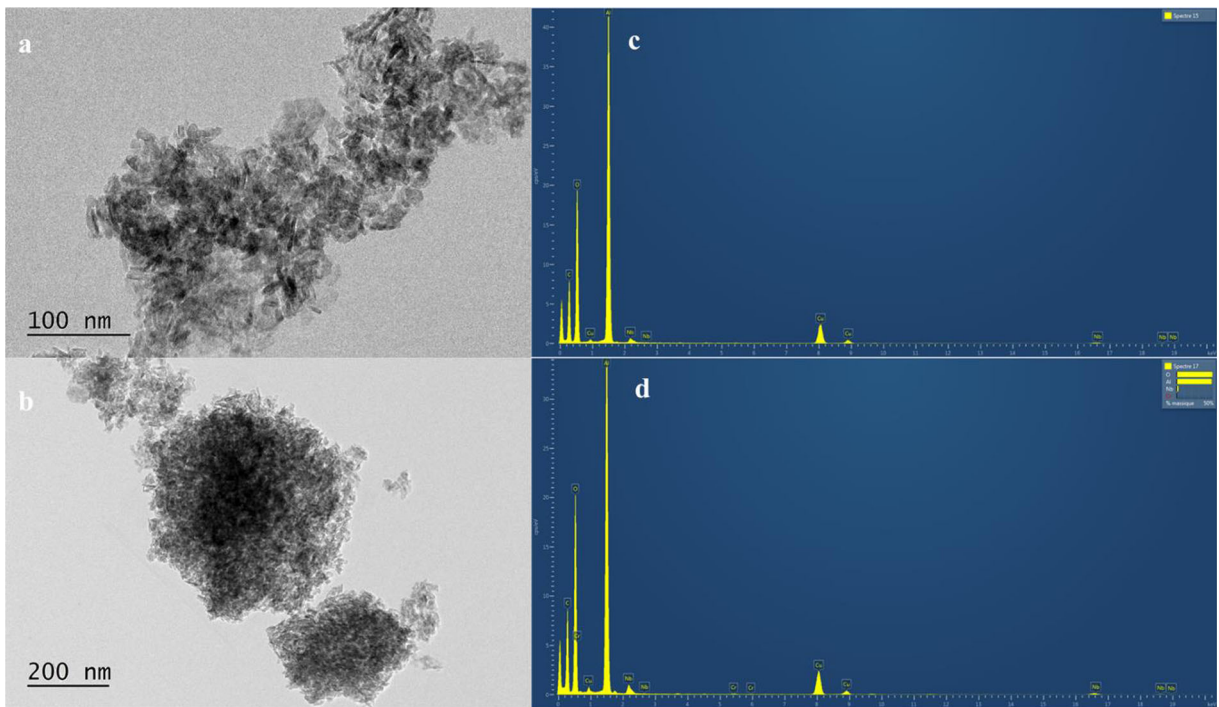


Fig. 10 a, b TEM images. c, d EDX spectra respectively for TEG 10 Al sample

added with various amounts of water are shown on Fig. 8. No visible trend in the evolution of the spectra with water content can be observed. Unlike commercial niobium HY 340, all of the synthesized materials have a

signal in the visible zone (between 400 and 700 nm). This signal may be caused by oxygen vacancies in the structure of the samples, giving them a caramel color, as reported by Brayner and Bozon-Verduraz (2003).

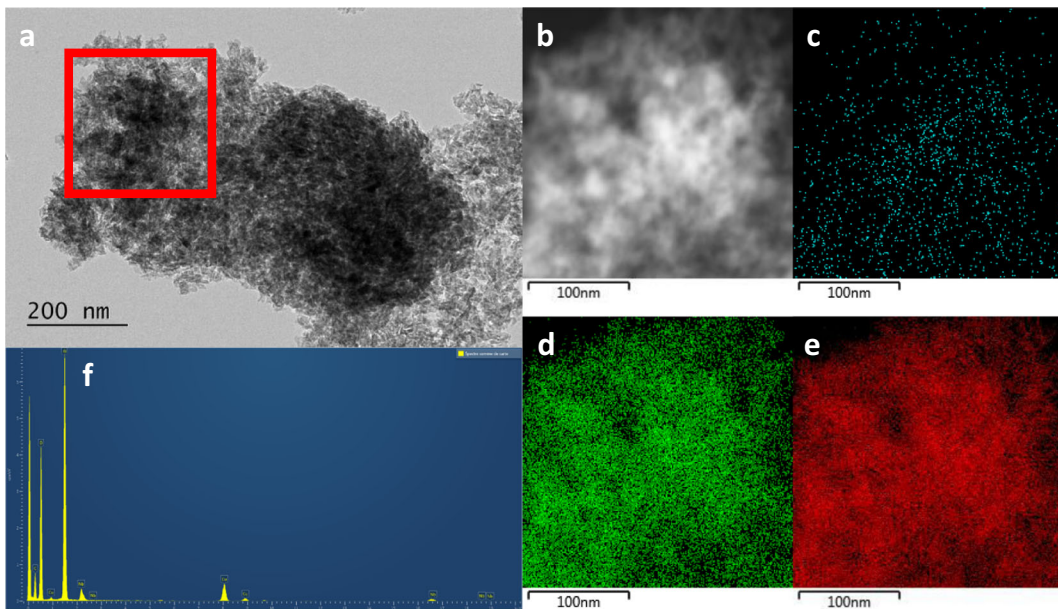


Fig. 11 a TEM and b STEM-HAADF images. STEM-EDX c Nb-L, d O-K, e Al-K maps. f EDX sum spectrum of the map for TEG 10 Al sample

Supported samples

Synthesis parameters for alumina-supported niobium oxide samples are reported in Table 1. These samples were characterized using XRD and HRTEM analyses to determine their morphologies. Table 3 shows the main characterization results obtained for these samples.

XRD profiles for the supported materials before calcination of all samples are the same as the one of NWA 155 (γ - Al_2O_3 phase). The phase of niobium formed could not be identified, either simply because the level was below the detection limit of the technique (the samples contain ca. 5 wt% of Nb_2O_5), or even because the high dispersion of the niobium oxide phase on the γ -alumina support result in the formation of a monolayer. In both cases, niobium phase could not be detected by means of an X-ray diffractometry.

The modification of the crystallinity of TTG 10 Al sample during calcination was investigated in situ using XRD (Fig. 9). Crystallization of Nb_2O_5 (pseudo-hexagonal phase, TT- Nb_2O_5) is observed 700 °C with the presence of two small peaks at 26.4° and 33.3° (corresponding to the peaks with relative intensity of 90 and 100%, respectively according to ICDD card 00-028-0317). This structure might appear because of sintering of the phase that contains niobium. Then, larger oxide particles are formed, which makes them detectable. After 900 °C, the two weak peaks associated with the Nb_2O_5 phase disappear, and new diffraction peaks are observed—29.4° and 33.7°—that can be assigned to the aluminum niobate (AlNbO_4) phase (ICDD card 00-26-030), showing the strong interaction of the active phase with the support. It shows that the active phase for evaluation tests is not the Nb_2O_5 , but the mixed oxide formed from this strong interaction. Moreover, at this temperature, a transition of the alumina phase from gamma to delta is observed.

Table 4 Concentration of Lewis acid sites of the alumina support (NWA 155) and of sample TTG 10 Al by IR spectroscopy of adsorbed pyridine

Sample	q_H (mmol/g)
NWA at 150 °C	68.0
NWA at 300 °C	32.1
TTG 10 Al at 150 °C	71.9
TTG 10 Al at 300 °C	22.6

In comparison with the TEG 10 sample (Fig. 6), the TEG 10 Al sample was analyzed by TEM (Fig. 10a, b) and EDX (Fig. 10c, d). The morphology of alumina is observed (Fig. 10 a, b). The EDX analysis proves the presence of niobium in both cases. The peak is small because we only have 5 wt% in niobium in the sample.

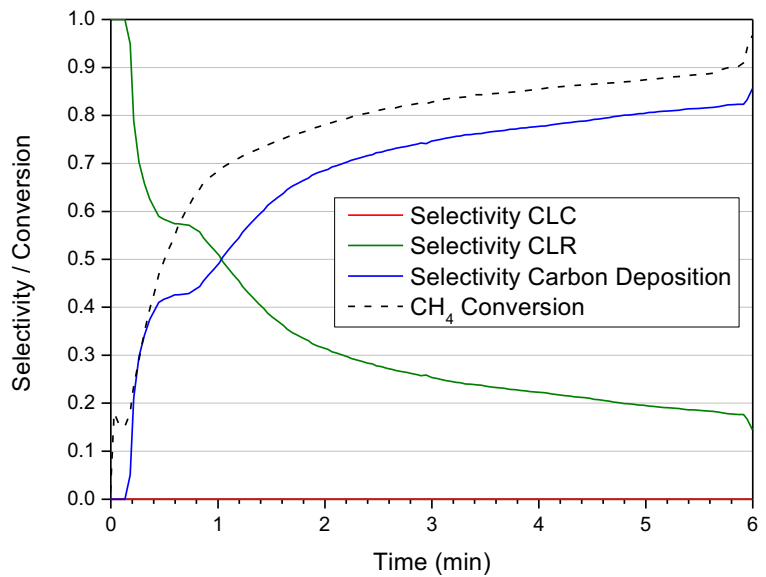
To better characterize the TEG 10 Al sample, STEM-HAADF and STEM-EDX map analyses were performed (Fig. 11). Figure 11 a shows the area that was analyzed. Figure 11b shows the STEM-HAADF result of the area that was chosen. Figure 11c–e show the mapping of the zone (11c (Nb-L), 11d (O-K), and 11e (Al-K)). It can be seen that niobium is well dispersed throughout the alumina (Fig. 11c) and finally Fig. 11f presents the EDX analysis result of the TEG 10 Al sample which shows the presence of the niobium peak.

Nitrogen physisorption results for the uncalcined samples are shown on Table 3. The surface area is practically the same as that of the alumina support (NWA 155). It is to be expected considering the low niobium loading in all samples.

Energy gap values of uncalcined samples are reported in Table 2 (samples prepared without alumina) and Table 3 (samples prepared with alumina). They were estimated using diffuse reflectance UV-Vis spectroscopy. The energy gap values for the synthesized samples are very close to those of commercial oxide HY 340 (3.3 eV). The energy gap values do not follow a clear trend and fluctuate from 3.2 to 3.7 eV depending on the sample. For sample TTG 00 Al, that did contain niobium, no energy gap value could be measured. A possible explanation for this is the presence of small amounts of polyol adsorbed on the surface of the materials.

The acidic properties of one of the supported samples (TTG 10 Al) were investigated by means of pyridine desorption detected by FTIR. Only Lewis acid sites were detected (band at 1454 cm^{-1}). The number of Lewis acid sites remaining after thermal treatment at 150 °C (corresponding to weak and strong Lewis sites) and after thermal treatment at 300 °C (corresponding to strong Lewis sites) are reported in Table 4 for TTG 10 Al and the alumina support alone (NWA 155 sample). Alumina alone and TTG 10 Al have similar acidities. The acidic properties of TTG 10 Al are therefore due mostly to its alumina component, and the small fraction of niobium added in this sample does not induce significant modification in the acidity.

Fig. 12 Fifth redox cycle for carrier DEG 10 Al C



Characterization results of supported niobium oxide presented in Table 3 showed that no significant differences were observed for different oxygen carriers. Differences have been observed only for non-supported oxides. Thus, only one of the oxygen carriers was selected to evaluations tests. To select this carrier, we considered the polyol cost and final temperature for reaction, assuming that costs for synthesis should be as low as possible. By these criterions, a good alternative is carrier DEG 10 Al C, prepared with diethylene glycol, the cheapest polyol among those studied here. Moreover, because of its high-water content, temperature during synthesis process was only 134 °C.

Fixed bed reactor evaluation

Figure 12 shows the results of reduction with 10% CH₄/Ar and oxidation with 10% O₂/Ar for DEG 10 Al C (DEG 10 Al calcined at 100 °C) sample. The result refers to the fifth redox cycle carried out with this material. For the reduction step (the first 6 min), as soon as the methane is sent, a large amount of H₂ is formed; together with CO and a small amount of water, unreacted methane is also present in the effluent. CO₂ is not produced during the reduction reaction.

After this reduction step, the reactor is purged under Ar during 5 min in order to remove all gases, and the

Fig. 13 Selectivity and conversion comparison for DEG 10 Al C during reduction step

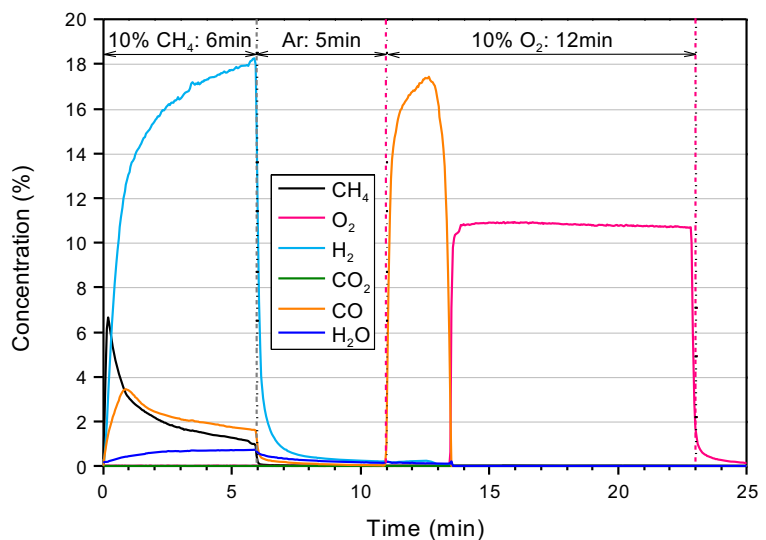
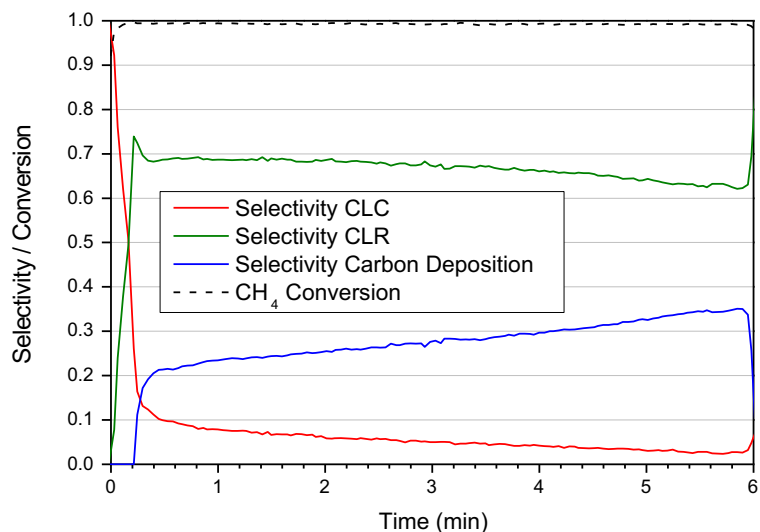


Fig. 14 Selectivity and conversion comparison for $\text{NiAl}_2\text{O}_4/\text{Al}_2\text{O}_3$ oxygen carrier during reduction step



oxidation step is started by flowing the O_2/Ar mixture on the sample. A large amount of CO is formed during the oxidation step. This shows that during the reduction step, a large amount of methane was converted into carbon deposit on the surface of the material and hydrogen was released. This reaction can be confirmed by the high H_2/CO ratio after the ten first seconds of reaction.

Selectivity curves for the Chemical-Looping Combustion (CLC) and Chemical-Looping Reforming (CLR) reactions and carbon deposit processes were constructed (see experimental part for details). These reactions are respectively represented by Eqs. 14, 15, and 16.

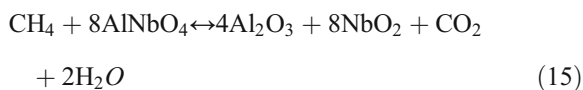
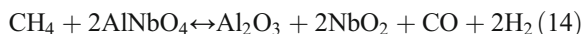


Figure 13 shows the selectivity and methane conversion results throughout the reduction step. During the first 10 s of reaction, the CLR process is completely selective although methane conversion is very low, reaching a maximum of 20% of the methane sent. After 10 s, the carbon deposit reaction increases gradually in prevalence and becomes the main reaction after 1 min time on stream.

Compared with other common oxygen carriers applied to chemical-looping reforming, this Nb-based carrier presented a different behavior. Zafar et al. (2005) studied Cu-, Mn-, Ni-, and Fe- oxides supported on SiO_2 as oxygen carriers. All of them start the reduction step by the production of CO_2 and steam; CO and H_2 are produced only after ca. 40 s under reductive conditions, when the oxidation of CH_4 to CO_2 is no longer total. Ni-based oxygen carrier showed the best reactivity.

Pröll et al. (2010) investigated the reactivity of Ni-based oxygen carrier on a 140-kW pilot plant. Results show that a mixture of CO_2 , H_2O , CO , and H_2 is expected from the fuel reactor stream in different conditions of air to fuel ratio.

Figure 14 shows the selectivity and conversion profile from a Ni-based oxygen carrier containing 19% of NiAl_2O_4 under the same conditions as described for Fig. 13. Preparation and characterization of such material were previously presented in (Barbosa et al. 2016). Conversion is almost total during all 6 min of reduction step. However, selectivity to CO_2 and H_2O formation is high at the beginning of reduction, with an increasing in syngas production selectivity a few seconds later. These results are in accordance with Zafar et al. (2005) and Pröll et al. (2010) as discussed here.

In the present work, we show that Nb-based oxygen carriers presenting AlNbO_4 as active phase can generate syngas from the beginning of reduction step without CO_2 formation. With an increasing of its reactivity, it could lead to an ideal operational condition where methane is totally converted to generate syngas, increasing the process yield.

Conclusions

Niobium oxide particles were prepared using the polyol method; most of the syntheses resulted in materials containing HNbO_3 . The crystalline structures vary widely with the water concentration in the system. The materials prepared with 10 mL of water had the clearest peaks on the X-ray diffraction profiles.

For the materials prepared in the presence of the alumina support Puralox NWA 155, AlNbO_4 was detected before calcination, indicating a strong interaction between niobia and alumina at high temperatures. When the reaction conditions of the CLR process are simulated, the process is totally selective toward CLR for the initial seconds of the reaction (no CLC products), a result that has never been published before. However, little methane is converted in this region, reaching a maximum of only 20%. After ca. 10 s time on stream, the conversion toward CLR progressively decreases due to the formation of coke. These are only preliminary results that show a great possibility of application for Nb-based oxygen carrier for CLR process.

Acknowledgements Pedro H.L.N.A dos Santos is grateful to Ciências Sem Fronteiras program from CNPq Brazil for financial support.

Compliance with ethical standards

Conflict of interest The authors declare that they have no conflict of interest.

References

- Adanez J, Abad A, Garcia-Labiano F, Gayan P, de Diego L (2012) Progress in chemical-looping combustion and reforming technologies. *Prog Energy Combust Sci* 38: 215–282
- Barbosa RD, Cruz GM, Santos PHLNA, Cortez GG, Rodrigues JAJ (2016) Nickel oxides supported on alumina as oxygen carriers for chemical-looping combustion and reforming of methane. *Appl Mech Mater* 830:30–37
- Barzetti T, Selli E, Moscotti D, Forni L (1996) Pyridine and ammonia as probes for FTIR analysis of solid acid catalysts. *J Chem Soc Faraday Trans* 92:1401–1407
- Brayner R, Bozon-Verduraz F (2003) Niobium pentoxide prepared by soft chemical routes: morphology, structure, defects and quantum size effect. *Phys Chem Chem Phys* 5:1457–1732
- Chun H, Kim D, Lim D, Lee W, Lee H (2010) A synthesis of CO-tolerant Nb_2O_5 -promoted Pt/C catalyst for direct methanol fuel cell; its physical and electrochemical characterization. *Int J Hydrog Energy* 35:6399–6408
- de Diego L, Gayán P, García-Labiano F, Celaya J, Abad A, Adanes J (2005) Impregnated $\text{CuO}/\text{Al}_2\text{O}_3$ oxygen carriers for chemical-looping combustion: avoiding fluidized bed agglomeration. *Energy Fuel* 19:1850–1856
- Emeis CA (1993) Determination of integrated molar extinction coefficients for infrared absorption bands of pyridine adsorbed on solid acid catalysts. *J Catal* 141:347–354
- Fiévet F, Brayner R (2013) The polyol process. In: Brayner R, Fiévet F, Cordin T (eds) *Nanomaterial: a danger or a promise?* Springer-Verlag, London, p 1–25
- Gayán P, de Diego L, García-Labiano F, Adanez J, Abad A, Dueso C (2008) Effect of support on reactivity and selectivity of Ni-based oxygen carriers for chemical-looping combustion. *Fuel* 87:2641–2650
- He J, Li Q, Fan Y (2013) Dispersion states and acid properties of SiO_2 -supported Nb_2O_5 . *J Solid State Chem* 202:121–127
- IUPAC Recommendations (1985) *Pure Appl Chem* 57:603
- IUPAC Recommendations (1994) *Pure Appl Chem* 66:173
- Kitano T, Shishido T, Teramura K, Tanaka T (2012) Brønsted acid property of alumina-supported niobium oxide calcined at high temperatures: characterization by acid-catalyzed reactions and spectroscopic methods. *J Phys Chem C* 116:11615–11625
- Ko E, Weissman J (1990) Structures of niobium pentoxide and their implications on chemical behavior. *Catal Today* 8:27–36
- Kvamsdal M, Jordal K, Bolland O (2007) A quantitative comparison of gas turbine cycles with CO_2 capture. *Energy* 32:10–24
- Li J, Lu G, Li K, Wang W (2004) Active Nb_2O_5 -supported nickel and nickel-copper catalysts for methane decomposition to hydrogen and filamentous carbon. *J Mol Catal A Chem* 221:105–112
- Li Y, Yan S, Yang W, Xie Z, Chen Q, Yue B, He H (2005) Effects of support modification on $\text{Nb}_2\text{O}_5/\alpha\text{-Al}_2\text{O}_3$ catalyst for ethylene oxide hydration. *J Mol Catal A Chem* 226:285–290
- Li S, Xu Q, Uchaker E, Cao X, Cao G (2016) Comparison of amorphous, pseudo-hexagonal and orthorhombic Nb_2O_5 for high-rate lithium ion insertion. *Crystal Eng Comm* 18:2532–2540
- Miracca I, Asen KAJ, Coulter C, Curran L, Lowe C, Moure G, Shlasner S (2009) The CO_2 capture project (CCP): results from phase II (2004–2009). *Energy Procedia* 1:55–62
- Mozer T, Passos F (2011) Selective CO oxidation on Cu promoted $\text{Pt}/\text{Al}_2\text{O}_3$ and $\text{Pt}/\text{Nb}_2\text{O}_5$ catalysts. *Int J Hydrog Energy* 36: 13369–13378
- Nowak I, Ziolk M (1999) Niobium compounds: preparation, characterization, and application in heterogeneous catalysis. *Chem Rev* 99:3603–3624
- Pröll T, Bolhár-Nordenkamp J, Kolbitsch P, Hofbauer H (2010) Syngas and a separate nitrogen/argon stream via chemical-looping reforming - a 140kW pilot plant study. *Fuel* 89: 1249–1256
- Tanabe K (2003) Catalytic application of niobium compounds. *Catal Today* 78:65–77
- Zafar Q, Mattisson T, Gevert B (2005) Integrated hydrogen and power production with CO_2 capture using chemical-looping

reforming - redox reactivity of particles of CuO, Mn₂O₃, NiO, and Fe₂O₃ using SiO₂ as a support. *Ind Eng Chem Res* 44:3485–3496

Zafar Q, Mattisson T, Gevert B (2006) Redox investigation of transition-state metals Ni, Cu, Fe and Mn supported on SiO₂ and MgAl₂O₄. *Energy Fuel* 20:34–44

Zhao Y, Zhou X, Ye L, Tsang S (2012) Nanostructured Nb₂O₅ catalysts. *Nano Reviews* 3:17631–17642

Ziolek M (2003) Niobium-containing catalysts - the state of the art. *Catal Today* 78:47–64

Publisher's note Springer Nature remains neutral with regard to jurisdictional claims in published maps and institutional affiliations.